Biochimica et Biophysica Acta 1788 (2009) 973–982

Contents lists available at ScienceDirect

Biochimica et Biophysica Acta

journal homepage: www.elsevier.com/locate/bbamem

Comparative modeling of the quaternary structure for the human TRPM8 channel and analysis of its binding features

Alessandro Pedretti, Cristina Marconi, Ilaria Bettinelli, Giulio Vistoli *

Dipartimento di Scienze Farmaceutiche "Pietro Pratesi", Facoltà di Farmacia, Università di Milano, Via Mangiagalli, 25, I-20133 Milano, Italy

ARTICLE INFO

Article history:
Received 10 August 2008
Received in revised form 24 January 2009
Accepted 4 February 2009
Available online 20 February 2009

Keywords:
TRPM8
Menthol
Icilin
Cold-sensitive ion channel
Homology modelling by fragment
Molecular docking

ABSTRACT

The aim of this study was to generate a reliable model for the homotetrameric structure of the human TRPM8 cation channel, a temperature sensor involved in innocuous cold perceptions. The described model was generated using a fragmental strategy and its interaction capacities were explored by docking a representative set of ligands. The analysis of the quaternary structure suggests that the N-terminus possesses a solenoidal topology which could be involved in tetramerization due to its electrostatic characteristics. Again, the tetramer model unveils a precise fitting between the segments of neighbouring monomers affording attractive suggestions for the multifaceted mechanism of channel gating. Docking results are in convincing agreement with mutational analyses and confirm that S4 and S4–S5 linker play a key role in channel activation. Overall, the proposed model could find fertile applications to further investigate the gating mechanism and to design truly selective ligands able to clarify the pathophysiological roles of the TRPM8 channel.

1. Introduction

Several natural products are able to induce cool or warm sensation. Thus, mint is well known for its ability to elicit a cold sensation, whereas pepper gives an opposite warm sensation. Such particular perceptions are due to the ability of their active ingredients (menthol for mint and capsaicin for pepper) to activate the transient receptor potential (TRP) superfamily of cation channels [1]. Among the known temperature sensors in nerve ending of mammals [2], TRP channels are characterized by a growing number of natural compounds which are able to stimulate them. Menthol and some related cyclic monoterpenes activate the TRP melastatin 8 receptor (TRPM8), a cold-sensitive ion channel, on which this study is focused [3]. Again, heat-activated TRP vanilloid 1 (TRPV1) is stimulated by capsaicin, the active ingredient of chili peppers, noxious cold-sensitive TRP ankyrin 1 (TRPA1) by pungent garlic oil, and heat-activated TRPV3 by camphor [4].

Until now, nine members of TRP family, which respond to varied temperature thresholds, have been described: TRPV1, TRPV2, TRPV3, TRPV4, TRPM2, TRPM4 and TRPM5 are heat-activated, whereas TRPM8 and TRPA1 are stimulated by cold [5]. In fact, the TRP channels are triggered by diverse chemical and physical stimuli and the precise mechanism of their activation is still unknown. Thus, TRPM8 is activated by cold temperature, ligands such as menthol and icilin (a synthetic derivative), positive membrane potential and the endogenous signalling lipid PIP2 [6].

More in detail, the *TRPM8* gene (also called *Trp-p8*), originally cloned as a prostate-specific protein, encodes for a 1104-residue transmembrane protein, whose functional quaternary structure is a homotetramer channel with modular structure and allosteric gating [7]. Although the cytoplasmic N-terminus represents more than half of the entire TRPM8 sequence, its role is still debated and recent evidences unveiled that amino acids 40–86 are required for localization to the plasma membrane [8]. Conversely, N-terminus should not play a significant role in tetramerization since the analysis of deletion mutants shows that the transmembrane domain is sufficient for TRPM8 assembly into tetramers.

The first four TM helices (termed S1–S4) of the transmembrane portion constitute the voltage sensor module and comprise the binding sites for menthol and icilin. Recent mutational analyses evidenced the critical role of protonated residues in S4 and S4–S5 linker, since their neutralization alter the gating charge, temperature sensitivity and menthol binding [9]. Similarly, mutagenesis studies unveiled that also S2 and S3 participate in binding of menthol and icilin, although such sites do not fully overlap, since most residues involved in menthol recognition are located in S2 [10], whereas icilin largely interacts with residues of S3 [11].

The last two TM helices (S5 and S6) and the connecting loop constitute the pore module, which is a non selective cation channel [12]. It is characterized by a highly conserved hydrophobic region and a conserved aspartate residue in the loop (Asp920), whose neutralization results in a non-functional channel. Moreover, S6 determines ion selectivity of TRPM8 as demonstrated by the introduction of positively charged residues, which switches from cation to anion selectivity [13].

* Corresponding author.
E-mail address: giulio.vistoli@unimi.it (G. Vistoli).

0005-2736/$ – see front matter © 2009 Elsevier B.V. All rights reserved.
doi:10.1016/j.bbamem.2009.02.007

The C-terminal domain, which includes the binding site for PIP2 and confers temperature sensitivity on TRPM8, appears also involved in tetramer stabilization since some mutations within the coiled coil region of C-terminus (978–1104) markedly reduce the ability of the TRPM8 monomers to form oligomeric channels [14]. Mutagenesis studies also revealed that activation by menthol involves a gating mechanism distinct and separable from that induced by cold, voltage or PIP2 [15].

TRPM8 is expressed in small diameter trigeminal and dorsal root ganglion neurons in which cooling and menthol evoke inward depolarizing currents and intracellular calcium rises. As also suggested by transgenic mice lacking TRPM8, it should be the cold sensor that confers to peripheral neurons their specific ability to respond to small temperature reductions, causing innocuous cold temperature sensations [16]. Furthermore, the activation of the TRPM8 channel has been reported to be involved in painful bladder syndrome, suggesting a possible role in the initiation of pain, as recently confirmed by the beneficial effects of AMTB, a selective channel blocker [17]. These evidences emphasize the relevance of deeply investigating structure and binding capacities of such a channel with a view to support its potential therapeutic applications.

Considering the above, we endeavoured to generate a full-length model for the human TRPM8 channel, analyzing its binding capacities with menthol, icilin as well as a set of known ligands including both natural and synthetic compounds. The monomer was generated by a fragmental strategy as recently proposed by us [18–21]. In detail, the transmembrane region was modeled exploiting its known homology with the mammalian voltage-dependent Shaker family K^+ channel [22], while the C-terminal domain was constructed using the experimental structure of HCN2 pacemaker channel as the template [23]. The obtained monomer was assembled in the corresponding homotetramer by protein–protein docking, and the final model was used in the mentioned docking analyses.

2. Computational methods

2.1. Generation of monomer structure

The construction of the monomeric structure of TRPM8 channel can be subdivided in three steps. The first part involved the modeling of vast cytoplasmic N-terminal domain by the classical homology techniques. The second step concerned the generation of the TM bundle by fragments using the structure of Shaker family K^+ channel [22] to guide the final assembly. Lastly, the C-terminus was modeled using the experimental structure of HCN2 pacemaker channel [23].

The amino acid sequence of human TRPM8 was retrieved from SwissProt Database (Entry name: TRPM8_HUMAN; accession number: Q7Z2W7). Globally, the protein was subdivided in 13 fragments as compiled in Table S3 (Supplementary data). The segments were separately predicted using LOMETS (http://zhang.bioinformatics.ku.edu/LOMETS), a local meta-threading-server for protein structure prediction [24]. For each segment LOMETS produces several realistic models and the preferred structure was chosen considering the following major conditions: (a) the predicted secondary structure from the sequence alignment, as obtained using ClustalX [25] (data not reported); (b) the lack of not predicted gaps; (c) the prediction score as calculated by LOMETS programs; (d) the helix conformation of the six transmembrane segments with characteristic slight bend of helices containing proline and glycine residues; (e) the global "U" shape for the loops in which the two ends are close enough to join to adjacent TM segments, and (f) the known homology between C-terminus and the HCN2 pacemaker channel.

The modeling of the vast N-terminus was a challenging task, which deserves a detailed description. Among the possible models proposed by LOMETS, the preferred result is based on the structure of importin-β (PDB Id.: 1QGR) [33]. This choice can be justified considering: (a) the marked agreement with the predicted secondary structure from the sequence alignment, as confirmed by a similarity percentage equal to 55.45% and an identity of 18.10%; (b) the very high prediction score; (c) the vast percentage of sequence modeled (86.1%) with few short unpredicted fragments; (d) the high structural quality of the proposed model with a percentage of residues falling in the allowed regions of the Ramachandran plot equal to 83.82%.

The second step of monomer construction involved the generation of the transmembrane bundle and the relative loops by fragments. Overall, this second part was less problematic since there is an experimental structure (i.e. the Kv1.2 Shaker channel, PDB Id.: 2A79), which can be successfully used to guide the assembly of the modeled fragments. As listed in Table S3, the exploited templates confirm that the TM segments can be modeled using small proteins characterized by a significant predominance of α-helices (e.g. actinin and catenin). Importantly, S3 and S4 transmembrane segments, which play a key role in channel activation, were predicted using the Kv1.2 Shaker channel, suggesting that these helices possess specific and conserved sequences, which cannot be found in other resolved proteins.

The long EL3 loop is predicted using a zinc-containing hydrolase and this result can be understood considering the ability of this segment to recruit cations, since this loop constitutes the extracellular entrance of the pore module. The other loops are predicted exploiting proteins with α/β mixed topology that, as in the case of haemagglutinin for CL2, are membrane glycoproteins with well-defined loop segments. Finally, the C-terminus was modeled using the HCN2J pacemaker as the template [23]. The folding is characterized by four α-helices (A, P, B, and C) with a β-roll between A and B helices.

The assembly of predicted fragments was performed superimposing the backbone of a fragment with that of the correspondent segment in the Kv1.2 Shaker channel and manually connecting the adjacent segments using VEGA software [26]. In detail, the superimposition involved the Cα atoms of transmembrane helices only, as the loops arrangement is clearly defined by the position of TMs, and their conformation was further relaxed by successive MD simulations (while the transmembrane bundle remains constrained during the molecular dynamics, as later described in next section). The terminal domains were manually added in the cytoplasmic side by minimizing the steric repulsion and maximizing the shape complementarity between solenoid architecture of N-terminus and globular folding of C-terminal domain.

Side chains and hydrogen atoms were added using VEGA. According physiological pH, Arg, Lys, Glu and Asp residues were preserved ionized, while His residues were considered neutral by default. After a careful visual scrutiny of obtained structure to avoid unphysical conditions, the model underwent an initial minimization until RMS = 1 to discard high-energy interactions, followed by a local minimization until RMS = 0.05, where all atoms were kept fixed except for those included within a 7.5 Å sphere around the manually connected bonds (at the fragment ends). Finally, the model was optimized by a final minimization made up by two phases: first a minimization without constraints until RMS = 0.1 and then a second minimization with backbone fixed until RMS = 0.01 to preserve the predicted structure.

2.2. Tetramer assembly

Since human TRPM8 possesses a homotetrameric structure, the obtained monomer was used to build the corresponding quaternary structure through protein–protein automatic docking using the EscherNG program [27]. The tetramer assembly is organized in two sequential steps. In the first step, two TRPM8 monomers were docked in order to obtain the corresponding homodimer, and then two dimers were docked together to generate the final TRPM8 tetramer. In detail, the z axis corresponds to transmembrane direction, the thickness of

the molecular slices was equal to 1.5 Å, the polygons were rotated with a step size of 20°, and 1000 possible solutions were globally produced. In both analyses, the best solution was selected considering: (1) the score of EscherNG, (2) the similarity with homotetrameric architecture of Kv1.2 Shaker channel, and (3) the accessibility of regions lining the solvent accessible pore module.

The obtained homotetramer underwent to a preliminary minimization followed by a molecular dynamics equilibration *in vacuo*. The simulation was carried out in 3 phases: 1) heating from 0 K to 300 K over 3000 iterations (3 ps, i.e. 1 K/10 iterations), 2) starting equilibration of 2500 ps, where the transmembrane backbone was kept fixed, and 3) equilibration of 7500 ps, in which the transmembrane backbone was harmonically restrained with decreasing harmonic force constants. More in details, harmonic force constant value was equal to 1 (1000 kJ mol^{-1} nm^{-2}) at the beginning of simulation and then was divided into two every 1.5 ns (then 5 MD were performed with harmonic force constant equal to 1, 0.5, 0.25, 0.12 and 0.06). Globally, the MD simulation lasted 10 ns and helices were correctly preserved also with harmonic force constant equal to 0.06. The last frame was used for the docking calculations after a final minimization until RMS = 0.01 (with harmonic force constant equal to 0.06).

The MD simulations had the following general characteristics: constant temperature at 300 ± 10 K by means of Langevin's algorithm; Lennard–Jones (L–J) interactions were calculated with a cut-off of 10 Å and the pair list was updated every 20 iterations; Newton's equation was integrated, using r-RESPA method, every 4 fs for long-range electrostatic forces, 2 fs for short-range non bonded forces, and 1 fs for bonded forces; a frame was stored every 5 ps, yielding 2000 frames. All calculations were carried out on a 16 CPU Tyan-VX50 system. The package Namd2.5 [28] was used with the force-field CHARMm v22 and Gasteiger's atomic charges. All minimizations in model construction and equilibration were performed using the conjugated gradients algorithm.

2.3. Docking simulations

Fig. 1 collects the small set of known TRPM8 ligands considered in the study including both agonists and antagonists [35]. The ligands structure was built using VEGA software, and the overall geometry and the atomic charges were optimized using MOPAC6.0. Their conformational profile was explored by a MonteCarlo procedure (as implemented in VEGA) which generated 1000 conformers by randomly rotating the rotors. All geometries so obtained were optimized and clustered according to similarity to discard redundant ones; in detail, two geometries were considered as non-redundant if they differed by more than 60° in at least one torsion angle.

The docking and scoring procedure involved extensive rigid-body sampling with the OpenEye Scientific Software package FRED (OpenEye Scientific Software, Santa Fe, NM, USA). Briefly, the FRED-based sampling was performed in 10 Å side box around Tyr745, whose key role in ligand recognition was confirmed by mutagenesis [10]. The obtained complexes were then refined focusing the minimization on the atoms inside a 10 Å sphere around the bound ligand.

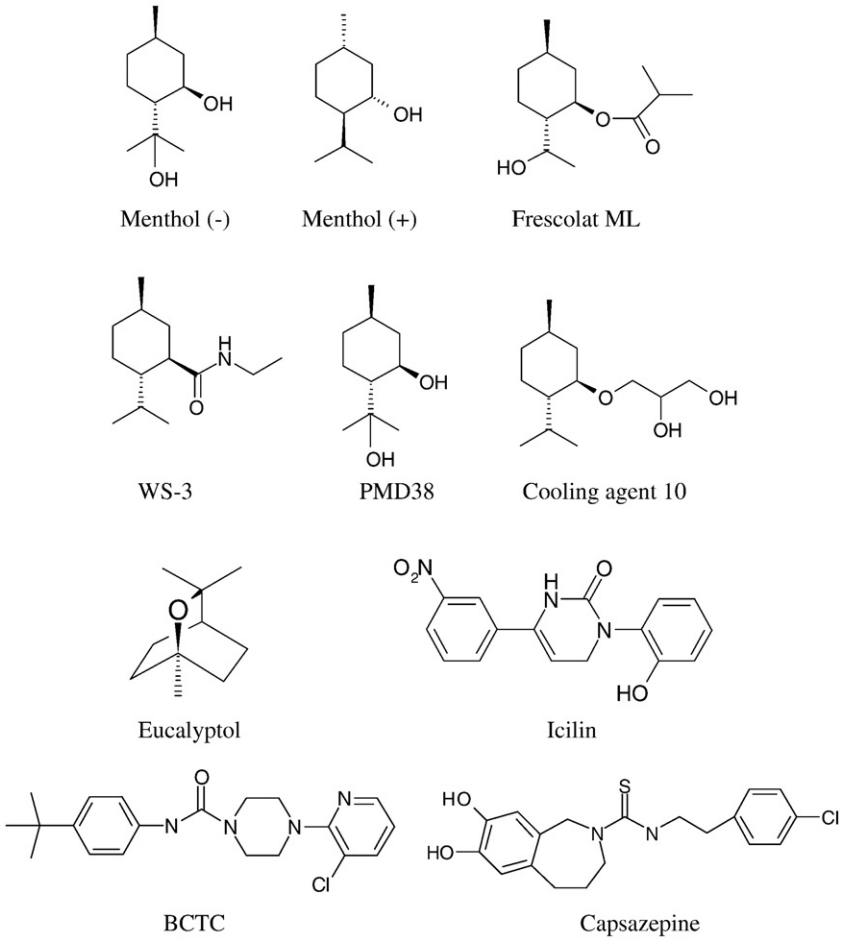

Fig. 1. TRPM8 ligands considered in docking simulations.

3. Results

3.1. Analysis of the TRPM8 monomer model

Fig. 2 reports the structure of TRPM8 monomer, coloured by segments, showing the classical elongated topology of such proteins with the transmembrane bundle being composed by six helices [29]. The soundness of the proposed model is assessed by the very high percentage (i.e., 80%) of residues falling in allowed regions of Ramachandran plot (as depicted in the inlet of Fig. 2). Overall, the monomeric model shows a significant abundance of helices, which represent about 60% of all monitored motifs. A bird's eye analysis of such model unveils that it can be roughly subdivided in two parts. The former corresponds to large cytoplasmic termini, where the C-terminus is arranged in the free space between the solenoidal shape of N-terminal domain and TM bundle. The latter includes the

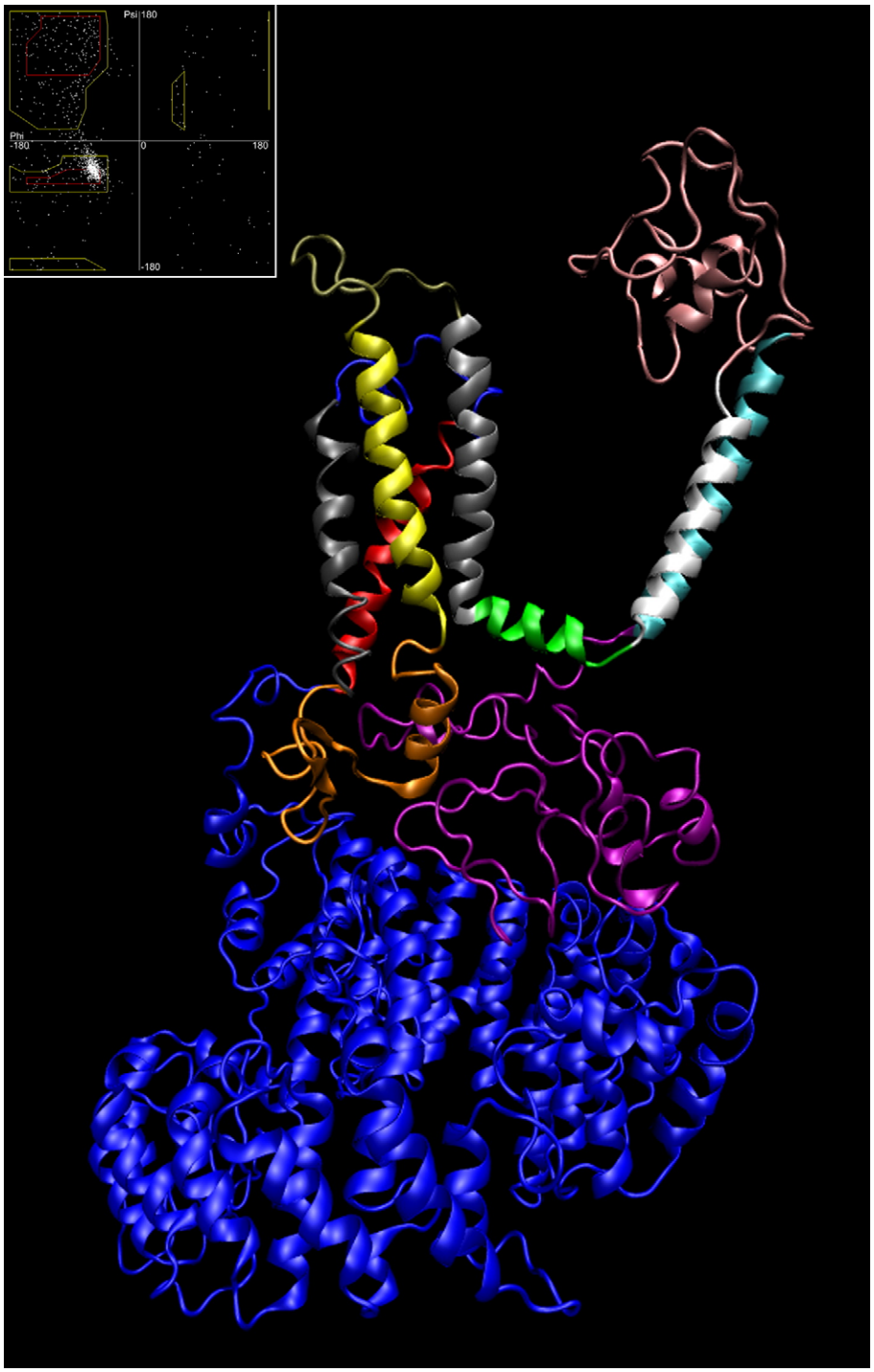

Fig. 2. Structure of the TRPM8 monomer coloured by segments (colour code: N-T: blue; S1: red; EL1: azure; S2: grey; CL1: brown; S3: yellow; EL2: gold; S4: grey; CL2: green; S5: white; EL3: pink; S6: azure; C-T: violet) showing the solenoid shape of very large N-terminal domain and the C-terminus which is packed between N-terminus and the transmembrane bundle composed by six helices (S1–S6). In the inlet, the Ramachandran plot for the model.

extracellular and cytoplasmic loops plus the transmembrane portion, where the two helices facing the pore (S5–S6) are visibly far from the first four voltage sensing helices (S1–S4).

3.2. The terminal domains

The modeling of the large N-terminus represented a quite arduous task, since reliable templates are unknown and the few available structure–function relations do not allow an easy prediction of its topology. Indeed, the unique well-established information is that the NT domains of all TRPMs are characterized by four regions of high homology (the so-called MHR regions) [30], while TRPC, TRPV, and TRPA channels contain ankyrin repeat units in their N-terminus. Moreover, recent experimental studies suggested that the NT segment of TRPM8 channels might be involved in plasma membrane localization.

Nonetheless, alignment analyses unveiled that the N-terminus of TRPM8 possesses significant homologies with the family of importin proteins [31], whose helicoidal structure is characterized by a large set of tandem repeats [32], which confer the typical shape and flexibility on such proteins. Analogously, the NT segment of TRPM8 comprises a set of repeat units, which characterizes the folding and, probably, the function of such domain. Specifically, the modeled N-terminus comprises 15 tandem repeat regions, whose parallel stacking defines a solenoidal right-handed super-helix, which can be subdivided in two valves having a global diameter about equal to 70 Å. The repeat units show a certain degree of structural variability. Indeed, most units show the classical folding composed by two antiparallel α-helices (HEAT repeat), some repeats are composed by three packed α-helices (Armadillo repeat), and, finally, some units, at the beginning of this domain, appear quite disordered being composed by one α-helix and one β-strand.

When considering the relative position of the mentioned MHR regions, one can observe that the first two MHR regions correspond to first valve, and are composed by the first seven repeat units, while the last two MHC regions constitute the second valve, which comprises the last seven repeats. The central eighth repeat is characterized by a large loop, which confers the flexibility on N-terminus, modulating the opening of the valves.

The analysis of structure–function relationships for the template (i.e. importin-β) [33] can afford some remarkable suggestions also for the functional role of N-terminus of TRPM8. Indeed, the importin proteins are characterized by conserved charged residues, which are organized so that the lateral parts are positively charged, while the central region is characterized by acidic residues. Crystallographic results evidenced that the interaction capacity and plasticity of importin proteins are mainly driven by such electrostatic gradients. Similarly, the NT domain of TRPM8 possesses a dipolarly distribution of charged residues, so that the first valve is mostly positively charged, whereas the second valve is largely negative, with a clear gradient in its electrostatic potential (as shown by MEP surface in Figure S1, Supplementary data). As later discussed, it is conceivable that the valves of four NT domains mutually interact in the homotetramer, exploiting their complementary electrostatic properties and, thus, stabilizing the quaternary structure.

The C-terminus of TRPM8 was modeled using the experimental structure of C-terminus for HCN pacemaker channel [23]. Like the template, the modeled C-terminal domain can be subdivided in two regions. The first part is mainly composed by α-helices separated by short loops, while, in the second domain, a β-roll comprises eight β-strands in a jelly-roll-like topology, which is typical of PIP2 binding site. The global folding of such CT domain is vastly constrained by abundant ionic interactions. In particular, the frequent basic residues may be involved in PIP2 interaction, whereas the hydrophobic coiled coil regions are involved in tetramerization contacting neighboring monomers (as later discussed).

3.3. The transmembrane bundle

The transmembrane bundle of TRPM8 shows the classical topology with six transmembrane helices (termed S1 trough S6) [29]. The first four helices (S1–S4) are involved in voltage sensing and harbour the binding sites for menthol and icilin, while the last two helices (S5–S6) are highly conserved and define the pore domain.

Table S2 (Supplementary data) compiles the inter-helix distances for the six TM segments, unveiling its subdivision in two clear-cut regions, which parallel the two functional roles of the TM bundle. Indeed, the former, which acts as voltage sensor, is composed by the first four helices, and shows a classical anticlockwise topology with a distance mean between helices equal to 11.75 Å. The latter, which lines the pore domain, is constituted by the last two helices, and reveals an antiparallel stacking with a distance equal to 9.44 Å. The two regions are significantly far with an average distance between them equal to 33.85 Å, and appear staggered with an angle equal about to 30°.

A deeper analysis of TM bundle reveals that S2 is the most peripheral helix having the widest distance with S5–S6, while S4 is the most central one as confirmed by its lowest distance with the pore helices. Finally, S1 and S3 occupy a lateral position showing a quite staggered arrangement in respect to S2 and S4. As mentioned in the Introduction, S2 and S3 are involved in the interaction with menthol and icilin, while S4 appears implicated in both binding and gating.

A closer examination of the voltage sensor reveals some features which deserve the reader's attention. Specifically, S2 and S3 helices are characterized by the critical binding roles of few polar residues (i.e. Tyr745 in S2, Asn799, Asp802, and Thr803 in S3) which are fully surrounded by hydrophobic residues with a significant predominance of aliphatic residues.

Again, S4 shows peculiar characteristics since it is markedly rich in conserved positively charged residues that, as recently demonstrated by mutational analyses, are involved in both binding and channel opening [9]. The positively charged groups also influence the conformational properties of this helix which can assume both canonical α helix and a more elongated 3_{10} helix maybe depending on the protonation and/or side-chain conformation of such positive residues. Importantly, Arg842 which is involved in both menthol binding and channel gating, is turned towards Tyr745 as also confirmed by the corresponding residues in the crystal structure of Kv1.2 channel and can indirectly interact with Tyr745 through the bridging action of Asp802.

Also the two helices lining the pore are markedly hydrophobic. More in detail, S5 is characterized by a set of parallel aromatic residues which face the pore and modulate the ion flux and also S6, which includes only apolar residues, can play a role in ion flux modulation since mutagenesis studies unveiled that the introduction of positive residues switches the channel from cation to anion selectivity [13].

The first two extracellular loops, connecting S1 to S2 and S3 to S4, are short arc-shape segments, whose folding is characterized by several conserved basic residues. They may be involved in both stabilizing interactions with phospholipidic heads and voltage sensing, since their conformation and ionization state may depend on the membrane potential. Although these two loops are sensibly far, they can interact due to the side chain of Tyr793 in EL2, which approaches the adjacent EL1 and contacts Lys715 and Lys722. It is plausible that such remarkable interaction, which strongly depends on the protonation of lysine residues, may influence the distance between EL1 and EL2, thus, modulating the accessibility of TM bundle.

The last extracellular loop, connecting S5 to S6, is markedly longer than the first two extracellular loops and shows a folding characterized by a mixed α/β topology stabilized by many polar interactions. Although in a recent model of TRPV1, this long loop was completely modeled in α helix [34], we preferred such a mixed topology which minimized the steric hindrances and allows the EL3 loop to be partially inserted in membrane region. Due to its size and arrangement, EL3

fully covers S5 and S6 helices, and, thus, modulates pore accessibility and ion flux as analyzed later in Discussion. Among the conserved charged residues, mutational studies revealed that Asp920 plays a key role in pH sensing, since its neutralization results in an inactive channel [12]. In our model, Asp920 faces the pore entrance and strongly interacts with both Arg890 and Arg897, thus justifying its relevance in defining folding and role of such loop. Moreover, other negatively charged residues in EL3 surround Asp920 and form a negative cluster which could be altered by protonation of Asp920 and could attract the cations.

The first intracellular loop is a very short segment packed between TM bundle and N-terminus. In contrast, the second cytoplasmic loop is a longer segment, which acts as a spacer to split the voltage sensor module (S1–S4) from the pore module (S5–S6). This segment assumes a distorted helix motif being perpendicular to S4, so that S4 and S5 appear spaced for about 25 Å. It is markedly hydrophilic mainly due to three basic residues, which tether its conformation and may be involved in channel activation.

3.4. Analysis of homotetramer complex

Fig. 3 shows the ribbon structure of the TRPM8 homotetramer (Fig. 3A: viewed from the extracellular side of the membrane, Fig. 3B: viewed parallel to the membrane), unveiling its fourfold symmetry with dimensions being approximately 176 Å × 165 Å × 140 Å. The tetramer also reveals its global conical shape with the cytoplasmic side being largely wider than the extracellular one.

Table S3 (Supplementary data) compares the surface values of each segment taken in the monomer alone with those obtained by the corresponding segment in the homotetramer. Clearly, the segments, which show the amplest surface diminution, are those mostly involved in interface definition and, thereby, in tetramer stabilization. The segments, whose surface remains virtually unchanged, include the first three transmembrane segments and the cytoplasmic loops, whereas the segments, whose surface markedly decreases in the tetramer, comprise the last three transmembrane segments as well as the extracellular loops.

Interestingly, the termini show a modest surface decrease, when computed in percentage, but their surface differences represent about one third of the total difference between monomer alone and homotetramer. This is due to the vast size of these segments, and, in particular, to the very large N-terminal domain, whose surface represents about 60% of the whole monomer surface. Recent studies evidenced that the terminal coiled-coil region of C-terminus is involved in tetramer stabilization since mutations in this region weaken the tetramer architecture [14]. The proposed model can explain these results since such a region contacts both the large N-terminus of the same monomer and the C-terminus of adjacent monomers.

The model suggests that also the N-terminus is implicated in tetramer stabilization and, indeed, the quaternary structure reveals that each NT domain contacts two adjacent N-termini and the interface is so structured that the positive side of an N-terminus contacts the negative regions of the adjacent domain. Although, the implication of N-terminus does not find experimental confirmation in the literature, it is impossible to exclude a possible role of this large segment also in tetramer stabilization as suggested by our model.

In the transmembrane bundle, the TM helices are finely arranged so that the two helices, lining the pore (S5 and S6) are partially fitted in the free space between the voltage-sensing module (S1–S4) and pore module (S5–S6) of neighbouring monomers. Such a precise architecture of TM bundle is confirmed by the surface differences, as compiled in Table S2. Indeed, the external helices of the voltage-sensing module (S1–S3) show a very modest decrease of surface area in tetramer, while the internal helix (S4) exhibits a significant decrease in surface value, because it contacts the pore module of adjacent monomer. Again, the pore facing helices (S5–S6) reveal the amplest surface diminutions, since they contact both the pore helices and S4 helix of the neighbouring monomers. The fine architecture of TM bundle and the precise contacts between TM helices of adjacent monomers allow to imagine how conformational shifts in the voltage-sensing module, due to the membrane potential or ligand interaction (see later in Discussion), could reflect in all tetramer amplifying the channel gating. Moreover, the precise interactions between transmembrane helices of adjacent monomers can explain why the transmembrane bundle alone is enough to induce the TRPM8 tetramerization as recently demonstrated.

Similarly, the large extracellular loop EL3 contacts the other EL3 segments defining the extracellular entrance of the pore as confirmed by Table S2. Such a particular arrangement emphasizes the pivotal role of EL3, which both modulates the channel opening and participates in quaternary structure stabilization. Conversely, the cytoplasmic loops, which are fully shielded by the large terminal domains, cannot contribute to the tetramer stabilization.

Taken globally, Fig. 3 and Table S3 emphasize that most TRPM8 segments are involved in homotetramer stabilization and reveal relevant contacts in (1) cytoplasmic portion due to the interactions between very large termini, (2) TM bundle, mainly due to the fitting between pore helices, and (3) extracellular region because of the pivotal packing of EL3 loop. Finally, only the cytoplasmic loops and the most external TM helices (S1–S3) are not involved in interface stabilization.

3.5. Docking studies on the menthol/icilin binding site

As a preamble, it is worth considering some relevant features of the putative binding site. All reported mutagenesis studies agree that Tyr745 (S2) plays a critical role in menthol binding, while icilin interacts with a wider pocket including also pivotal residues in S3 (Asn799, Glu802, Gly805). Recent mutagenesis studies unveiled that positively charged residues in S4 and in the S4–S5 linker (i.e. Arg842 and Lys856) are implicated in menthol binding and channel activation [9]. A bird's eye analysis of the binding site reveals that Tyr745 interacts with Asp802 and faces a very apolar cavity characterized by several aliphatic residues in S2 (Val742, Val743, Phe744, Ile746, Ala747, Phe748, Leu749, Leu750, and Leu806). Based on these premises and with a view to explore the interaction capacities of binding site harboured by voltage-sensing module (S1–S4), a small set of known TRPM8 ligands (Chart 1) were docked into the described model [35].

Fig. 4A shows the putative complex between menthol and TRPM8. Conceivably, the main interaction stabilizing the complex is the H-bond between Tyr745 and the ligand's hydroxy group, while the mentioned apolar residues are involved in hydrophobic contacts with the skeleton of menthol molecule. Specifically, the methyl group contacts Val742 and Val743, the isopropyl moiety lines Leu749 and Leu750, and, finally, the cyclohexyl ring lies on Ile746.

Since the menthol molecule has only one polar function and Arg842 is visibly far from Tyr745 (distance about 11.2 Å), one can argue that Arg842 could not directly interact with the ligand, but it could be involved in the stabilization of binding site. However, the proposed model suggests that Arg842 can contact Thr745 through the bridging role of Glu802, so that it is conceivable that the side chain of Arg842 could be influenced by the bound menthol in the cavity.

Furthermore, the precise complementarity of the apolar contacts between menthol and binding site can justify the ligand stereo-specificity, since in the complex between menthol(+) and TRPM8 the methyl group clashes against Val742 and Val743, while the isopropyl moiety cannot contact Leu749 and Leu750. Globally, these results emphasize the key role of both the hydrophobic interactions elicited by methyl and isopropyl groups and the suitable arrangement of hydroxy function as indeed confirmed by very low activity of menthone and cyclohexanol [36].

The menthol derivatives yield docked complexes very similar to that of menthol confirming the key roles played by the mentioned interactions. In particular, the complex with the menthyl lactate (Frescolat) shows that the ester carbonyl group interacts with Tyr745, while the hydroxy function contacts Asp802, suggesting that Tyr745 acts as H-bonding donor in the ligand binding. Also the carbamate derivative WS-3 affords a similar docking result, since the amide carbonyl group interacts with Tyr745 while the ethyl chain contacts Leu806. This may mean that the agonists are able to break the polar interactions between Tyr745 and Asp802 and the implications of this

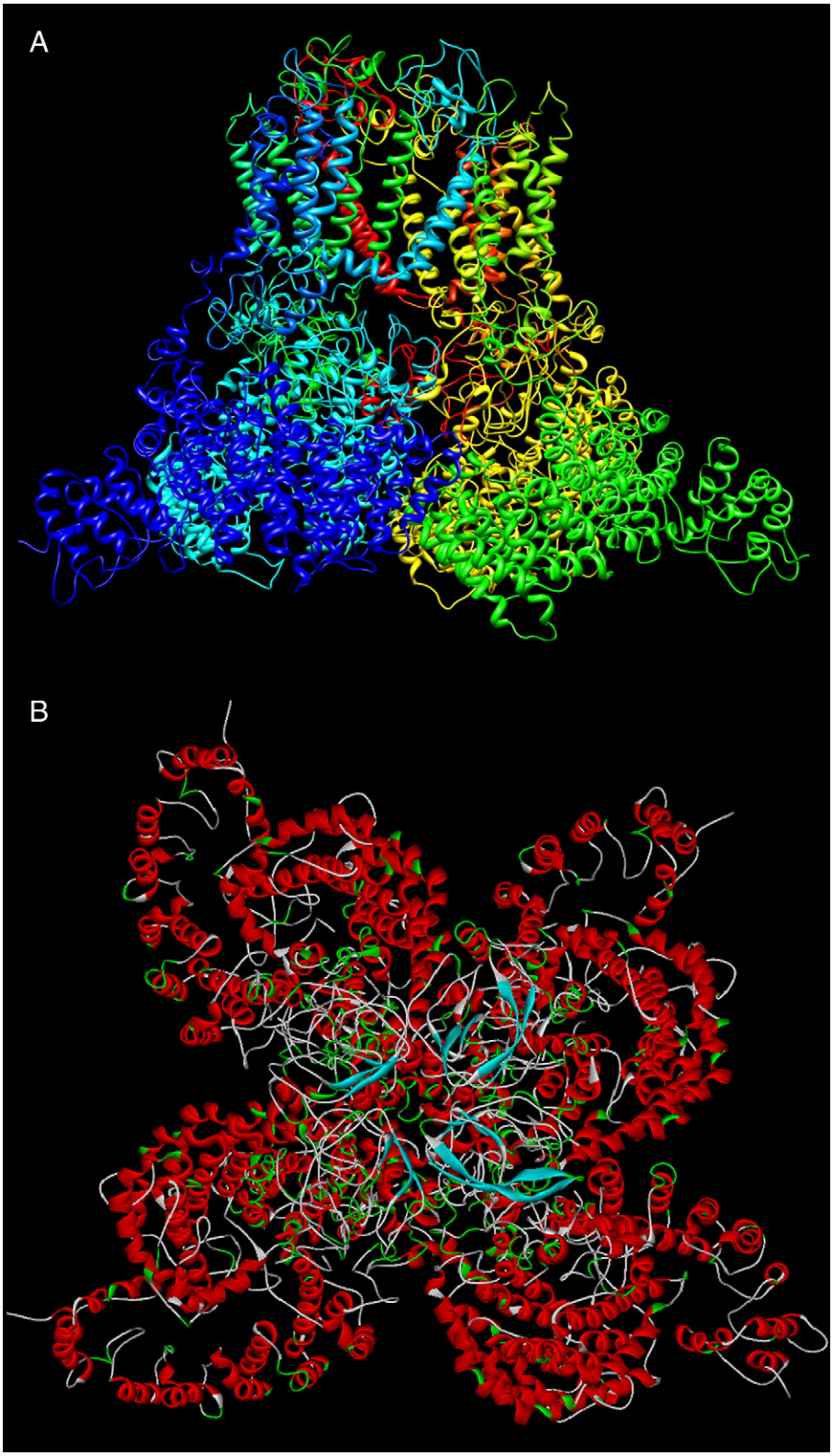

Fig. 3. Model for the homotetramer structure. (A) model viewed parallel to the membrane and coloured by segment. (B) viewed from the extracellular side and coloured by secondary structure (legend: red and green = helices, azure = sheet, and white = random coils).

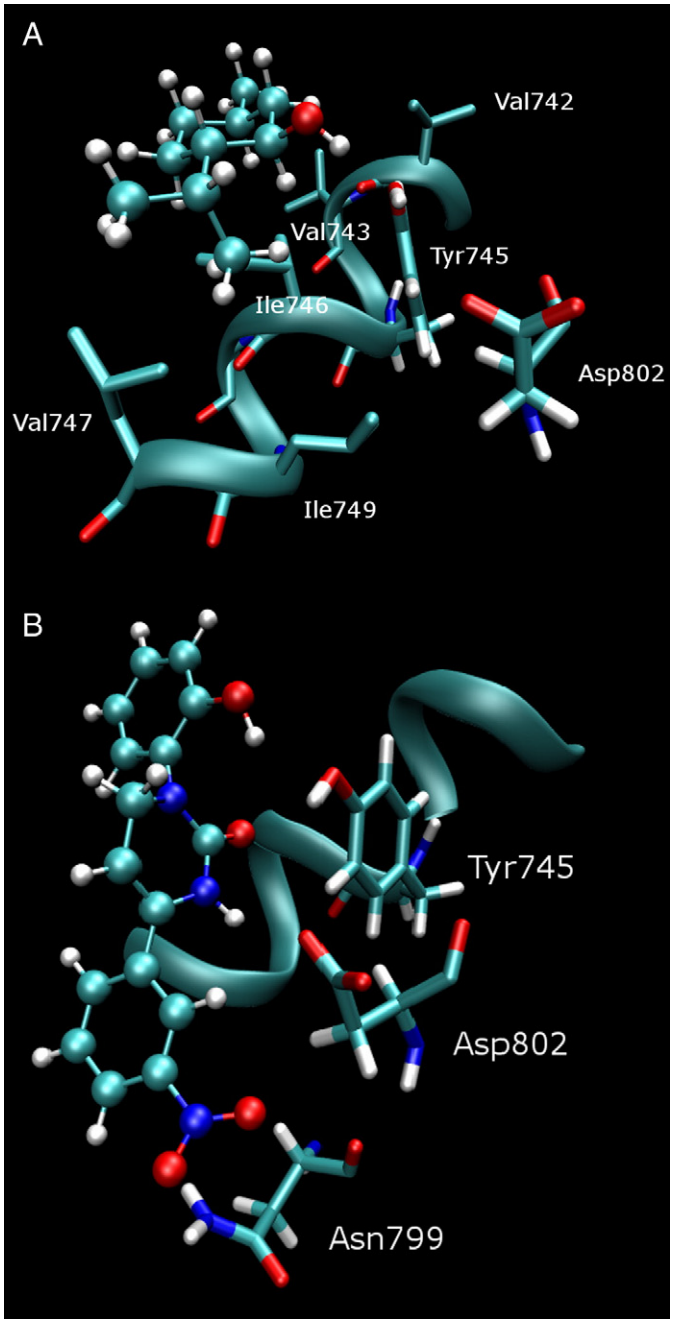

Fig. 4. Main interactions stabilizing the putative complexes between TRPM8 model and menthol (3A) and icilin (3B). In both complexes, one can note the key interaction between ligand and Tyr745 and the major role played by hydrophobic contacts realized by apolar residues in S2.

evidence will be analyzed in the Discussion. Finally, the lower potency of PMD-38 emphasizes the relevance of hydrophobic contacts which are clearly weakened by the second hydroxy group which cannot realize any polar interactions.

Fig. 4B depicts the putative complex between ilicin and TRPM8, showing that the phenol ring replaces the menthol's cyclohexanol ring stabilizing H-bond with Tyr745. Again the lactamic function of the dihydropyrimidin-2-one ring interacts with Asp802 and the nitrophenyl ring contacts Asn799. The reported interactions are in clear agreement with mutational data which suggested that Asp802 and Asn799 play a key role in icilin binding [11]. In fact, mutagenesis studies enlightened that also Gly805 has a critical role in icilin binding, even if docking result suggest that this residue does not contact directly the ligand but is located in a very constrained region so that its mutation with a necessarily bulkier residue distorts the fine architecture of binding site.

Noticeably, icilin is a quite symmetric molecule so that one can suppose that such a ligand can also assume an overturned pose in which the nitrophenyl moiety replaces the menthol scaffold contacting Tyr745 and the phenol ring interacts with Asn799. Both poses realize a quite identical interaction pattern although docking scores suggest that the binding mode depicted in Fig. 4B is the preferred one. The two considered antagonists show putative complexes similar to that of ilicin. In particular, both antagonists occupy the menthol's cavity with moieties which realize successful hydrophobic interactions but are unable to contact Tyr745 and the lesser potency of capsazepine could be ascribed to two hydroxy functions which cannot interact with Tyr745 and weaken the apolar contacts. Similarly, the antagonists occupy the region near to Asn799 without interacting with this residue.

Table 1 compiles the potency values (expressed in μM) as well as the docking score functions, as computed by Fred, which afforded the best correlations with bioactivities. Interestingly, the two considered score functions are: (1) Shapegauss, which mainly accounts for shape complementarity, and (2) Zapbind, which accounts for the polar interactions, being based on a combination of surface contact terms and Poisson–Boltzman energy approximations (as computed by ZAP module [37]). Such relationships confirm the key role of both precise hydrophobic contacts (as encoded by Shapegauss scores) and key polar interactions (as described by Zapbind function), which trigger the channel opening.

4. Discussion

The mechanism of TRPM8 activation and, more in general, the mechanism of thermoTRP channel gating is still a debated question although some recent evidences can somewhat clarify the main characteristics of the channel opening. Indeed, a very important and recent mutational analysis unveiled the critical role of Arg842 and Lys856 in S4 and S4–S5 linker for menthol sensitivity and gating charge suggesting that the mechanisms with which menthol and voltage influence channel opening are quite superimposable. The authors also proposed a quantitative 8-state MWC model in which the four subunits undergo a concerted voltage dependence transition between the open and close state [9].

Furthermore, a recent study unveiled that voltage alone induces a submaximal stimulus and that ligands produce voltage-independent gating. These evidences may indicate a certain degree of modularity in the channel opening suggesting that the mechanisms of ligands and voltage are not fully coincident [38]. Overall these studies emphasized the critical role of S4 helix that, as recently demonstrated for voltage-dependent phosphatase, undergoes a conformational shift during the channel activation ranging from the standard α helix to a more

Table 1
Bioactivities and docking scores for the compounds considered in docking study.

Compound	Potency (EC_{50}–IC_{50})[a]	Shapegauss score[b]	Zapbind score[b]
Menthol (−)	4.1	−113.15	−10.87
Menthol (+)	14.4	−82.51	−8.25
Icilin	0.2	−240.14	−18.03
Cooling agent 10	6.00	−158.57	−14.79
Frescolat ML	3.3	−160.42	−13.27
WS3	3.7	−144.22	−12.95
PMD38	31	−93.67	−9.67
Eugenol	7700	−56.45	−7.69
BCTC	0.8	−143.88	−24.10
Capsazepine	18	−111.67	−23.23

[a] Expressed in μM.
[b] Expressed in Kcal/mol.

elongated 3–10 helix suggesting that the gating may involve a possible elongation of the S4 segment [39]. The proposed role of S4 is also in line with the evidence that the pore opening does not involve conformational changes in S5 or S6 being based on a rigid-body movement of the entire pore module [40].

Starting from these evidences, the proposed TRPM8 model was exploited to shed light on possible molecular mechanisms able to account for both menthol sensitivity and voltage sensing. Fig. 5A shows the geometric relations between menthol binding cavity and S4 plus S4–S5 linker. One can note that Arg842 is placed between Glu802 and Asp835 and probably it can interact with such negative residues changing the conformation of its side chain. Moreover, the ion-pair between Arg842 and Glu802 may be influenced by Tyr745 and then by the interaction between this latter and ligands. The particular arrangement of these residues seems to suggest that Arg842 can move between Glu802 and Asp835 depending on ligand binding and/or voltage and such a transition may influence the S4 structure. Considering our model, one can suppose that the ligand binding breaks the interaction between Tyr745 and Glu802 favoring that between Arg842 and Glu802, which implies a down movement of Arg842 and the shift of S4 segment to 3–10 helix. This may mean that the menthol binding induces a local change in S3 which approaches Asp802 to S4 promoting the contact between Arg842 and Asp802.

A similar role may be claimed for Lys856 which belongs to S4–S5 linker but is turned towards S4 helix with which can form clear polar interactions. The particular conformation of such a residue may suggest that it could act as a pillar which assures the proper arrangement between S4 and S4–S5 linker thus stabilizing the α helix conformation. One can suppose that the voltage can destabilize such a tethering effect promoting the shift towards a more elongated 3–10 helix. Even if the mutagenesis studies suggest a possible implication of Lys856 in menthol binding, the model seems to exclude a direct interaction between this residue and ligands. Although Lys856 may stabilize the precise architecture of the binding cavity, the model suggests that it plays a principal role in channel gating.

Globally, these considerations may suggest that: (i) the close state is characterized by S4 in canonical α helix, while the open state requires its elongation to 3–10 helix; (ii) in the close state Arg842 interacts with Asp835 stabilizing the α helix conformation in the S4 helix; (iii) in the close state Glu802 is turned towards S2 and interacts with Tyr745; this interaction is broken when the ligand interacts with Tyr745; (iv) the open state requires a transition of Glu802 towards S4, so that it can attract Arg842 which, in turn, leaves Asp835; (v) such a shift of Arg842 unblocks the S4 conformation, which assumes the elongated 3–10 helix. Such observations propose that the open state involves an elongation of S4 which induces a joint movement of S4–S5 linker and, more importantly, the opening of S5–S6 pore. The described mechanism could be triggered also by voltage, which can influence the arrangement of charged residues and/or by pH of milieu which can change the ionization state of considered charged residues.

With a view to verify the reported hypotheses, the putative open state for a single monomer was built by changing the conformation of S4 helix. We do not know which S4 residues are involved in this conformational shift, but conceivably it should imply the residues after Asp835 and then we changed the folding of Asp835–Arg851 segment moving consequently S4–S5 linker and the pore helices. Fig. 5B shows the superimposition of the close and open states highlighting the different arrangement of pore helices.

A more in-depth analysis of Fig. 5B reveals that the transition from α helix to 3–10 motif in the S4 segment induces a downstream S4 elongation of about 4–5 Å and such a shift reduces the angle between S4 and S4–S5 linker which range from 89° to 80°. Consequently, the pore helices vary their slope of about 16°, as measured for S5. Such a change induces a widening of pore entrance of about 9 Å per monomer. Such a movement of the pore helices reflects on the large EL3 extracellular loop, which contacts the other two extracellular loops. In particular, the open state is characterized by a clear ion-pair that Glu906 realizes with Lys719 which can contribute to the open state stabilization. Noticeably, the distance between these two charged residues range from 14 Å in the close state to 3 Å in the open state underlining that very small folding variations in S4 can induce remarkable structural changes in the pore entrance.

Such a mechanism can also account for the modularity of channel opening which may depend on the extension of the S4 helix which

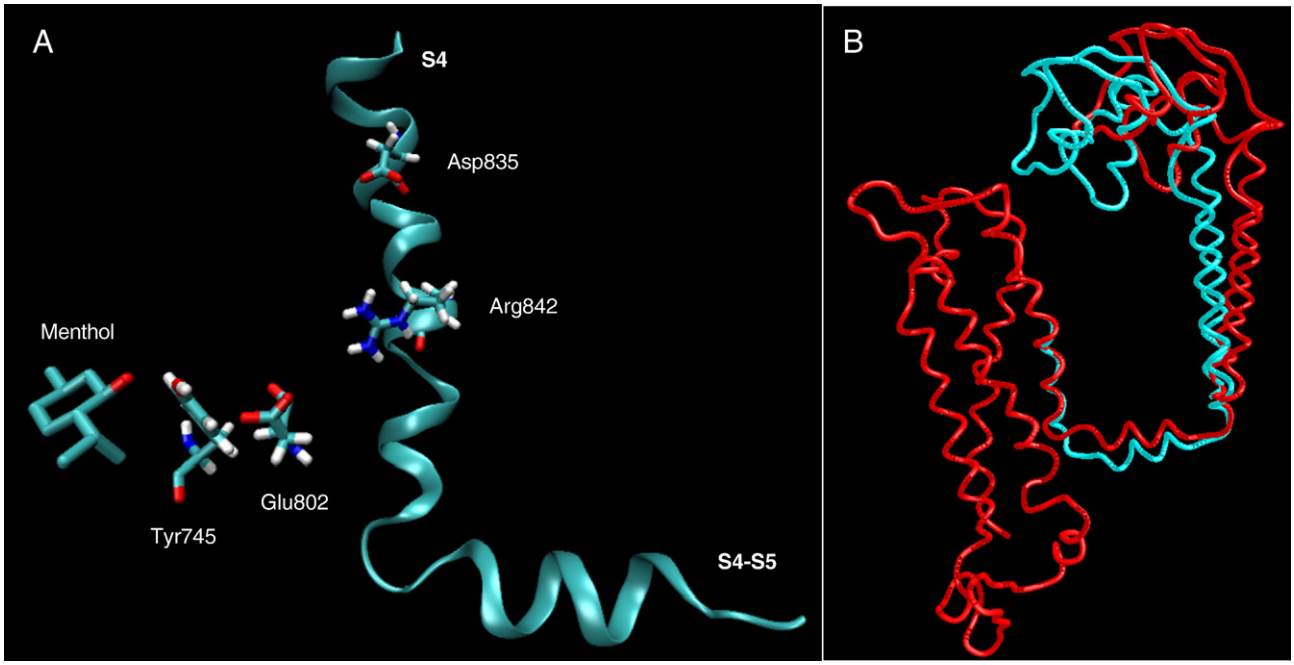

Fig. 5. Possible mechanism for channel opening. (A) geometric relations between ligand, Tyr745 and crucial residues in S3. (B) Comparison between open state (azure) and close state (red). One can observe that the principal differences between the two states is the conformation of S4 which is more elongated in the open state and this shift reflects on pore helices which shows a slope which corresponds to a channel opening.

shifts to 3–10 helix. Considering that ligands can induce a maximal stimulus and hypothesizing that they induce the conformational change for the Asp835–Arg851 (17 residues) segment, one can calculate that each residue, which shifts to 3–10 helix, widens the pore entrance of about 0.5 Å changing the pore helices slope of about 1°. For example, the neutralization of Lys856, which normally interacts with His845, could free the helix conformation of the His845–Arg851 inducing a channel gating which is about an half of maximal opening.

5. Conclusion

The study presents a homology model for TRPM8 tetramer exploring the interaction capacities of the menthol binding site as well as its implications for channel opening. The study also proposes a possible mechanism for channel activation based on a conformational shift which could occur in the S4 helix. Clearly the model cannot account for all experimental data and, for example, the binding and functional roles of C-terminus were somewhat disregarded to focus the reader's attention on the structural characterization of the transmembrane bundle.

Even considering the limitations of docking analyses mainly due to possible flexibility of transmembrane helices which cannot be accounted for by a static homology model, the structural quality, the consistency of modeled complexes and the ability to account for many experimental evidences afford a convincing verification for the here proposed TRPM8 model giving a clear picture for its homotetrameric folding. Also in this study, the fragmental approach proved successful in modeling complex transmembrane proteins. In detail, this study confirmed that such an approach can be very useful (1) to fill the structural gaps, modeling segments for which reliable templates are still unknown (as in the case of N-terminus of TRPM8), and (2) to profitably combine more known templates in order to generate full-length models. Although our efforts to corroborate the homology modeling by fragments will continue in the future by modeling increasingly complex transmembrane proteins, the TRPM8 model further confirms the versatility of such an approach to generate fertile models for any transmembrane proteins. The in-depth investigation of the therapeutic opportunities of such TRPM8 channel requires highly selective ligands and the here proposed model appears very useful for this purpose being well suited to rational ligand design and/or virtual screening.

Appendix A. Supplementary data

Supplementary data associated with this article can be found, in the online version, at doi:10.1016/j.bbamem.2009.02.007.

References

[1] K. Venkatachalam, C. Montell, TRP channels, Annu. Rev. Biochem. 76 (2007) 387–417.
[2] C. Belmonte, F. Viana, Molecular and cellular limits to somatosensory specificity, Mol. Pain 4 (2008) 14.
[3] T. Voets, G. Owsianik, B. Nilius, TRPM8, Handb. Exp. Pharmacol. 179 (2007) 329–344.
[4] G. Appendino, A. Minassi, A. Pagani, A. Ech-Chahad, The role of natural products in the ligand deorphanization of TRP channels, Curr. Pharm. Des. 14 (2008) 2–17.
[5] G. Reid, ThermoTRP channels and cold sensing: what are they really up to? Pflugers Arch. 451 (2005) 250–263.
[6] B. Nilius, F. Mahieu, Y. Karashima, T. Voets, Regulation of TRP channels: a voltage–lipid connection, Biochem. Soc. Trans. 35 (2007) 105–108.
[7] R. Latorre, S. Brauchi, G. Orta, C. Zaelzer, G. Vargas, ThermoTRP channels as modular proteins with allosteric gating, Cell Calcium 42 (2007) 427–438.
[8] C.B. Phelps, R. Gaudet, The role of the N terminus and transmembrane domain of TRPM8 in channel localization and tetramerization, J. Biol. Chem. 282 (2007) 36474–36480.
[9] T. Voets, G. Owsianik, A. Janssens, K. Talavera, B. Nilius, TRPM8 voltage sensor mutants reveal a mechanism for integrating thermal and chemical stimuli, Nat. Chem. Biol. 3 (2007) 174–182.
[10] M. Bandell, A.E. Dubin, M.J. Petrus, A. Orth, J. Mathur, S.W. Hwang, Patapoutian, High-throughput random mutagenesis screen reveals TRPM8 residues specifically required for activation by menthol A, Nat. Neurosci. 9 (2006) 493–500.
[11] H.H. Chuang, W.M. Neuhausser, D. Julius, The super-cooling agent icilin reveals a mechanism of coincidence detection by a temperature-sensitive TRP channel, Neuron 43 (2004) 859–869.
[12] B. Nilius, J. Prenen, A. Janssens, G. Owsianik, C. Wang, M.X. Zhu, T. Voets, Regulation of the Ca2+ sensitivity of the nonselective cation channel TRPM4, J. Biol. Chem. 280 (2005) 22899–22906.
[13] F.J. Kühn, G. Knop, A. Lückhoff, The transmembrane segment S6 determines cation versus anion selectivity of TRPM2 and TRPM8, J. Biol. Chem. 282 (2007) 27598–27609.
[14] I. Erler, D.M. Al-Ansary, U. Wissenbach, T.F. Wagner, V. Flockerzi, B.A. Niemeyer, Trafficking and assembly of the cold-sensitive TRPM8 channel, J. Biol. Chem. 281 (2006) 38396–38404.
[15] S. Brauchi, G. Orta, C. Mascayano, M. Salazar, N. Raddatz, H. Urbina, E. Rosenmann, F. Gonzalez-Nilo, R. Latorre, Dissection of the components for PIP2 activation and thermosensation in TRP channels, Proc. Natl. Acad. Sci. U. S. A. 104 (2007) 10246–10251.
[16] A. Dhaka, T.J. Earley, J. Watson, A. Patapoutian, Visualizing cold spots: TRPM8-expressing sensory neurons and their projections, J. Neurosci. 28 (2008) 566–575.
[17] E.S. Lashinger, M.S. Steiginga, J.P. Hieble, L.A. Leon, S.D. Gardner, R. Nagilla, E.A. Davenport, B.E. Hoffman, N.J. Laping, X. Su, AMTB, a TRPM8 channel blocker: evidence in rats for activity in overactive bladder and painful bladder syndrome, Am. J. Physiol. Renal Physiol. 295 (2008) 803–810.
[18] A. Pedretti, M. Villa, M. Pallavicini, E. Valoti, G. Vistoli, Construction of human ghrelin receptor (hGHS-R1a) model using a fragmental prediction approach and validation through docking analysis, J. Med. Chem. 49 (2006) 3077–3085.
[19] A. Pedretti, G. Vistoli, Modeling of human ghrelin receptor (hGHS-R1a) in its close state and validation by molecular docking, Bioorg. Med. Chem. 15 (2007) 3054–3064.
[20] A. Pedretti, L. De Luca, C. Sciarrillo, G. Vistoli, Fragmental modeling of human glutamate transporter EAAT1 and analysis of its binding modes by docking and pharmacophore mapping, ChemMedChem 3 (2008) 79–90.
[21] A. Pedretti, C. Marconi, C. Bolchi, L. Fumagalli, R. Ferrara, M. Pallavicini, E. Valoti, G. Vistoli, Modelling of full-length human α4β2 nicotinic receptor by fragmental approach and analysis of its binding modes, Biochem. Biophys. Res. Commun. 369 (2008) 648–653.
[22] S.B. Long, E.B. Campbell, R. Mackinnon, Crystal structure of a mammalian voltage-dependent Shaker family K+ channel, Science 309 (2005) 897–903.
[23] W.N. Zagotta, N.B. Olivier, K.D. Black, E.C. Young, R. Olson, J.E. Gouaux, Structural basis for modulation and agonist specificity of HCN pacemaker channels, Nature 425 (2003) 200–205.
[24] S. Wu, Y. Zhang, A local meta-threading-server for protein structure prediction, Nucleic Acids Res. 35 (2007) 3375–3382.
[25] J.D. Thompson, T.J. Gibson, F. Plewniak, F. Jeanmougin, D.G. Higgins, The ClustalX windows interface: flexible strategies for multiple sequence alignment aided by quality analysis tools, Nucleic Acids Res. 24 (1997) 4876–4882.
[26] A. Pedretti, L. Villa, G. Vistoli, VEGA: a versatile program to convert, handle and visualize molecular structure on Windows-based PCs, J. Mol. Graph. 21 (2002) 47–49.
[27] L. De Luca, A. Pedretti, G. Vistoli, M.L. Barreca, L. Villa, P. Monforte, A. Chimirri, Analysis of the full-length integrase–DNA complex by a modified approach for DNA docking, Biochem. Biophys. Res. Commun. 310 (2003) 1083–1088.
[28] L. Kalé, R. Skeel, M. Bhandarkar, R. Brunner, A. Gursoy, N. Krawetz, J. Phillips, A. Shinozaki, K. Varadarajan, K. Schulten, NAMD2: greater scalability for parallel molecular dynamics, J. Comput. Phys. 151 (1999) 283–312.
[29] G.M. Clayton, S. Altieri, L. Heginbotham, V.M. Unger, J.H. Morais-Cabral, Structure of the transmembrane regions of a bacterial cyclic nucleotide-regulated channel, Proc. Natl. Acad. Sci. U. S. A. 105 (2008) 1511–1515.
[30] D.E. Clapham, TRP channels as cellular sensors, Nature 426 (2003) 517–524.
[31] A. Cook, F. Bono, M. Jinek, E. Conti, Structural biology of nucleocytoplasmic transport, Annu. Rev. Biochem. 76 (2007) 647–671.
[32] M.A. Andrade, C. Perez-Iratxeta, C.P. Ponting, Protein repeats: structures, functions, and evolution, J. Struct. Biol. 134 (2001) 117–131.
[33] G. Cingolani, C. Petosa, K. Weis, C.W. Muller, Structure of importin-beta bound to the IBB domain of importin-alpha, Nature 399 (1999) 221–229.
[34] G. Fernández-Ballester, A. Ferrer-Montiel, Molecular modeling of the full-length human TRPV1 channel in closed and desensitized states, J. Membr. Biol. 223 (2008) 161–172.
[35] H.J. Behrendt, T. Germann, C. Gillen, H. Hatt, R. Jostock, Characterization of the mouse cold-menthol receptor TRPM8 and vanilloid receptor type-1 VR1 using a fluorometric imaging plate reader (FLIPR) assay, Br. J. Pharmacol. 141 (2004) 737–745.
[36] D.D. McKemy, W.M. Neuhausser, D. Julius, Identification of a cold receptor reveals a general role for TRP channels in thermosensation, Nature 416 (2002) 52–58.
[37] N.V. Prabhu, P. Zhu, K.A. Sharp, Implementation and testing of stable, fast implicit solvation in molecular dynamics using the smooth-permittivity finite difference Poisson–Boltzmann method, J. Comput. Chem. 25 (2004) 2049–2064.
[38] J.A. Matta, G.P. Ahern, Voltage is a partial activator of rat thermosensitive TRP channels, J. Physiol. 585 (2007) 469–482.
[39] C.A. Villalba-Galea, W. Sandtner, D.M. Starace, F. Bezanilla, S4-based voltage sensors have three major conformations, Proc. Natl. Acad. Sci. U. S. A. 105 (2008) 17600–17607.
[40] N. Bocquet, H. Nury, M. Baaden, C. Le Poupon, J.P. Changeux, M. Delarue, P.J. Corringer, X-ray structure of a pentameric ligand-gated ion channel in an apparently open conformation, Nature 457 (2009) 111–114.